

Abstract. We consider a sample of 22 nearby clusters of galaxies observed with the Medium Energy Concentrator Spectrometer (MECS) on board *BeppoSAX*. They cover the range in gas temperature between 3 and 10 keV, with bolometric X-ray luminosity between 2×10^{44} erg s⁻¹ and 6×10^{45} erg s⁻¹. Using the de-projected gas temperature and density profiles resolved in a number of bins between 5 and 7 and obtained from this dataset only, we recover the total gravitating mass profiles for 20 objects just applying the (i) spherical symmetry and (ii) hydrostatic equilibrium assumptions. We investigate the correlations between total mass, gas temperature and luminosity at several overdensities values and find that the slopes of these relations are independent of the considered overdensity and consistent with what is predicted from the cluster scaling laws. The best-fit results on the normalization of the $M - T$ relation are slightly lower, but still consistent considering the large errors that we measure, with hydrodynamical simulations. A segregation between relaxed and non-relaxed systems is present in each plane of these relations pointing out a significant component in their intrinsic scatter. This segregation becomes more evident at higher overdensities and when physical quantities, like M_{gas} and L , that are direct functions of the amount of gas observed, are considered.

Key words: galaxies: cluster: general – galaxies: fundamental parameters – intergalactic medium – X-ray: galaxies – cosmology: observations – dark matter.

Gravitating mass profiles of nearby galaxy clusters and relations with X-ray gas temperature, luminosity and mass

S. Ettori¹, S. De Grandi², and S. Molendi³

¹ European Southern Observatory, Karl-Schwarzschild-Str. 2, D-85748 Garching, Germany

² Osservatorio Astronomico di Brera, Via Bianchi 46, I-23807 Merate (LC), Italy

³ Istituto di Fisica Cosmica “G.Occhialini”, Via Bassini 15, I-20133 Milano, Italy

Received 24 February 2002 / Accepted 7 June 2002

1. Introduction

The amplitude and the shape of the power spectrum of the primordial density fluctuations on scales of about $20 h_{50}^{-1}$ Mpc can be effectively constrained with the mass function of galaxy clusters. Since the early '90s, X-ray observations have been used to build large datasets of measured luminosities and, with more effort because a larger number of source counts is required, temperatures of the X-ray emitting plasma trapped in the cluster gravitational potential. These observed quantities are expressions of the physical processes that are taking place in the galaxy clusters and manifest the energy and the mass of these systems. Then, comparing the observed distribution in luminosity (or temperature) with theoretical models of the expected cluster number density that are functions of total mass and redshift and depend upon the cosmological model adopted (e.g. Press & Schechter 1974), it has been possible to put constraints in the “normalization–shape” plane of the primordial density fluctuations spectrum (see, e.g., the pioneering work of Henry & Arnaud 1991 and the most recent results in Ikebe et al. 2002 and references therein).

However, the conclusions reached making this comparison rely on an efficient way to relate the observed quantities (like gas luminosity and temperature) to the gravitating mass of the systems. Gas–dynamics simulations (e.g. Evrard, Metzler & Navarro 1996, Schindler 1996) have confirmed the expected correlation between mass and temperature and have shown that mass estimates are reliable when obtained through X-ray analysis under the assumption of spherical symmetry and hydrostatic equilibrium. More recently, mass profiles obtained relaxing the condition of plasma isothermality have shown a significant mismatch in normalization and slope of the mass–temperature relation between observational data and simulations (e.g. Horner, Mushotzky & Scharf 1999, Nevalainen, Markevitch & Forman 2000). On the other hand, it has been clear since the first compilation of catalogues of luminosity and temperature (Mushotzky 1984, Edge & Stewart 1991) that the observed correlation between these two quantities deviates significantly from the expected scaling law, suggesting contribu-

tions to the total energy of the plasma from physical phenomena other than the gravitational collapse.

The observed Luminosity–Temperature ($L - T$) and Mass–Temperature ($M - T$) relations for galaxy clusters are, therefore, the foundation to construct the cluster mass function and to use these virialized objects as cosmological probes. In this paper, we investigate these relations and, more in general, any correlation between observed and inferred quantities using *BeppoSAX* observations of 22 nearby clusters of galaxies with resolved gas temperature and density profiles. The main differences between this study and previous work on the same subject are:

1. the use of *BeppoSAX* data that allows us to extend the analysis of spatially-resolved spectra up to $20'$ in radius, i.e. ~ 2.5 times the most favourable configuration with *Chandra* (Weisskopf et al. 2000) and to put under control some systematic effects (e.g., sharper and more energy-independent Point-Spread-Function than the *ASCA* one –Tanaka et al. 1994–, more stable and lower background than the one observed in *XMM-Newton* –Jansen et al. 2001),
2. the direct deprojection of the spectral results to reconstruct the gas temperature and density profiles in a model-independent way.

The sample presented in this work is, to date, the largest for which the physical quantities (i.e. gas density, temperature, luminosity, total mass, etc.) have all been derived simultaneously from spatially-resolved spectroscopy of the same dataset. The difference between this approach and others which make use of data coming from different satellites and/or make strong assumptions on the temperature profiles, such as isothermality, is twofold: on one side the use of data from different missions and the simplistic assumptions on the temperature profiles allow to build up samples bigger than ours, on the other they increase the likelihood of systematic effects which may in turn affect the relations between the observed quantities.

The paper is organized as follows: in Section 2, we describe the *BeppoSAX* MECS observations of the galaxy clusters in our sample and the results of the spectral analysis considered in this work; the deprojection technique applied to the projected spectral results is discussed in Sect. 3; the gravitating mass profiles

are obtained and compared with the optical measurements in Section 4; in Section 5, we study the correlation between the total mass, gas temperature, gas mass and luminosity; we summarize our results and present our conclusions in Sect. 6.

All the errors quoted are at 1σ level (68.3 per cent level of confidence for one interesting parameter) unless otherwise stated. The cosmological parameters $H_0 = 50h_{50}^{-1} \text{ km s}^{-1} \text{ Mpc}^{-1}$ and $\Omega_m = 1 - \Omega_\Lambda = 1$ are assumed hereafter.

2. The sample

We selected from the *BeppoSAX* SDC archive all the on-axis pointings of galaxy clusters with redshift smaller than ~ 0.1 and exposure times larger than 30 ksec. The observation log for the cluster sample, with a detailed discussion of the metal abundance and temperature profiles derived for subsets of this sample, is given in De Grandi & Molendi (2001 and 2002, hereafter DGM02).

In this paper we discuss data from the imaging Medium-Energy Concentrator Spectrometer (MECS; 2-10 keV; Boella et al. 1997). The MECS consists of two identical grazing incidence telescopes with imaging gas scintillation proportional counters in their focal planes. The field of view of the MECS is circular with radius of $\sim 25'$. This detector has a spectral resolution of $\sim 8\%$ at 6 keV and a Point Spread Function (PSF) of $\sim 1'$ (HPR), which varies only weakly with the energy (D'Acri, De Grandi, & Molendi 1998). The MECS has an entrance Beryllium window sustained by a thicker supporting structure, or strongback, in form of a circular ring and four ribs, which has transmission properties different by the rest of the window.

The data analysis is fully described in De Grandi & Molendi (2001, 2002), hence in this paper we will only summarize the whole procedure. Standard reduction procedures and screening criteria have been applied using the SAXDAS package under the FTOOLS environment to produce equalized and linearized MECS event files. Each cluster has been divided into concentric annuli centered on the X-ray emission peak computed by fitting a Gaussian to the photon distributions in both the x - and y -direction on *ROSAT* PSPC images; out to $8'$ we accumulate spectra from four annular regions each $2'$ wide; beyond this radius we accumulate spectra from annuli $4'$ wide. The energy dependent PSF of the MECS and the energy-dependent telescope vignetting for on-axis observations have been taken into account in our extended sources analysis by generating appropriate instrument response files (with the *ef-ffarea* program available within the SAXDAS package) to be used when fitting the accumulated spectra. We have computed the corrected effective area for the $8' - 12'$ annulus, which is covered by the circular region of the strongback, by considering the typical thickness of the strongback and its transmission as a function of the energy and position. All other regions of the detector covered by the strongback have been appropriately masked and the data rejected. The background subtraction has been performed using spectra extracted from blank sky events files in the same regions of the detectors as the source.

We fitted each spectrum with a single-temperature plasma in collisional equilibrium at the redshift of the cluster (MEKAL model –Kaastra 1992, Liedhal et al. 1995– in XSPEC v. 10.0 –Arnaud 1996), absorbed by the nominal Galactic column density (*wabs* model; Dickey & Lockman 1990).

3. Deprojection of the spectral results

The physical quantities constrained from fits of spectra with counts collected from cluster regions projected on the sky need to be converted to their values in the spherical shells that constitute the assumed spherical geometry of the X-ray emitting plasma. Fitting a thermal model to a projected spectrum provides, for each annulus, (i) an estimate for the Emission Integral, $EI = \int n_e n_p dV = 0.82 \int n_e^2 dV$, through the normalization K of the model, $K = \frac{10^{-14}}{4\pi d_{\text{ang}}^2 (1+z)^2} EI$ (see MEKAL model in XSPEC; we assume $n_p = 0.82n_e$ in the ionized intra-cluster plasma); (ii) a direct measurement of the emission-weighted gas temperature, T_{ring} (note that the observed temperature is properly a photon-weighted temperature, but the difference from our assumed definition is completely negligible), metal abundance, Z_{ring} , and luminosity, L_{ring} . The purpose of the deprojection is, for example, to recover the value of the gas temperature in shells, $T_{\text{shell}} \equiv T_i$, that is defined as

$$T_{\text{ring}} \equiv T_j = \frac{\sum_{i=\text{outer shell}}^{i=j} T_i w_{ij}}{\sum_{i=\text{outer shell}}^{i=j} w_{ij}} \quad (1)$$

where $w_{ij} = L_i \times \text{Vol}(i, j) / \text{Vol}(i) = \epsilon_i \text{Vol}(i, j)$ provides the luminosity for a given shell i with volume $\text{Vol}(i)$ weighted by the part of this volume projected on the ring j , $\text{Vol}(i, j)$. Using this notation, it is simple to note that $L_{\text{ring}} \equiv L_j = \sum_{i=\text{outer shell}}^{i=j} \epsilon_i \text{Vol}(i, j) = \sum_{i=\text{outer shell}}^{i=j} w_{ij}$.

From Kriss, Cioffi & Canizares (1983; see also McLaughlin 1999 and, particularly relevant to X-ray analysis, Buote 2000), the volume shell observed through each ring adopted in the spectral analysis can be evaluated and a matrix, \mathbf{Vol} , can be built with components equal to the parts the volume of the shells (rows i) seen at each ring (or annuli; column j).

The deprojected physical quantities can be then obtained through the following matrix products (shown by the symbol $\#$):

$$\begin{aligned} n_e &= \left[(\mathbf{Vol}^T)^{-1} \# (EI/0.82) \right]^{1/2} \\ \epsilon &= (\mathbf{Vol}^T)^{-1} \# L_{\text{ring}} \\ \epsilon T_{\text{shell}} &= (\mathbf{Vol}^T)^{-1} \# (L_{\text{ring}} T_{\text{ring}}) \\ \epsilon Z_{\text{shell}} &= (\mathbf{Vol}^T)^{-1} \# (L_{\text{ring}} Z_{\text{ring}}), \end{aligned} \quad (2)$$

where $(\mathbf{Vol}^T)^{-1}$ indicates that the matrix is firstly transposed and then inverted. The emission due to the shells projected along the line of sight but with the corresponding annuli outside the field-of-view is taken into account with an edge correction factor estimated assuming a power law distribution of the emission proportional to r^{-4} (cfr. equation A8 in the appendix of McLaughlin 1999). Finally, we have to assign a single radius, r_{ave} , to each shell. Formally, for each shell delimited from

the radii r_i and r_{i+1} , this radius should be the one that solves the equation $n_{\text{gas}}^2(r_{\text{ave}}) = 3/(r_{i+1}^3 - r_i^3) \int_{r_i}^{r_{i+1}} n_{\text{gas}}^2(r) r^2 dr$. Considering that (i) $n_{\text{gas}}^2(r) \propto r^{-\alpha}$ with α that has generally a value enclosed between 3 and 6 and can also vary between these values as function of radius in the same cluster, and (ii) complicated iterative procedure and interpolation are required (see, e.g., discussion about equation A9 in the appendix of McLaughlin 1999), we have checked that the assumption of $r_{\text{ave}} = (r_{i+1} + r_i)/2$ is consistent with analytic solution of the equation above for an acceptable α within 2 per cent.

We have applied this technique to the single-phase results of the spectral analysis presented in DGM02. In rings where part of the flux was masked for the presence of point-sources, we correct the normalization K by the relative amount of area not considered implicitly assuming spherical symmetry.

For each cluster, we finally have the following outputs: gas bolometric luminosity in each shell, $L \equiv L_{\text{shell}}$; gas temperature in each shell, $T \equiv T_{\text{shell}}$; electron density in each shell, n_e , and, integrating it over the volume, the gas mass, M_{gas} . An error is assigned to each quantity given the distribution of the values after 100 Monte-Carlo simulations obtained from scattering the original projected input with respect to their Gaussian error.

Following DGM02, we divide our sample into two groups of objects with (CF; 12 clusters) and without (NCF; 10 clusters) a cooling flow in the central region (see reviews in Sarazin 1988, Fabian 1994), according to the mass deposition rate quoted in Peres et al. (1998; NCF systems have a deposition rate consistent with zero; cf. Table 1). It is worth noticing, however, that this classification is meant to distinguish between relaxed (CF) and not-completely-relaxed (NCF) systems. In fact, also considering recent results from *Chandra* (David et al. 2001, Ettori et al. 2002, Sanders & Fabian 2002, Johnstone et al. 2002) and *XMM-Newton* (Tamura et al. 2001, Molendi & Pizzolato 2001, Matsushita et al. 2002) analyses of nearby clusters that show a lack of spectroscopic evidence of multi-phase gas, we parameterize all the X-ray emission with a single temperature model.

4. X-ray estimate of the gravitational mass profiles

To estimate the total gravitating mass, M_{tot} , we make direct use of the deprojected gas temperature and electron density values estimated from the spectral best-fit with a single phase model. For each cluster, we select the mass model that reproduces better the deprojected gas temperature profile inverting the equation of the hydrostatic equilibrium between the dark matter potential and the intracluster plasma:

$$-G\mu m_p \frac{n_e M_{\text{tot,model}}(<r)}{r^2} = \frac{d(n_e \times kT)}{dr} \quad (3)$$

where $\mu=0.6$ is the mean molecular weight in a.m.u., G is the gravitational constant, m_p is the proton mass, and using the deprojected electron density, n_e . As mass models, we consider two functional forms obtained from the integration of the following dark matter density profile: (i) the King approximation to the isothermal sphere (King 1962, Binney & Tremaine

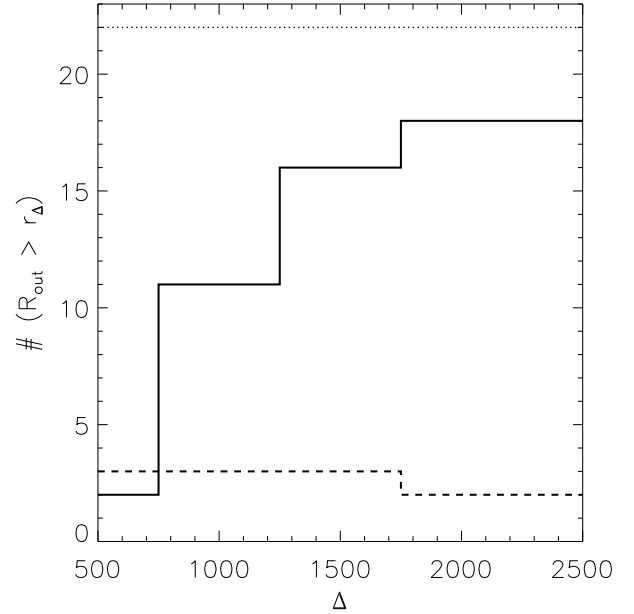


Fig. 1. Histograms of the number of objects considered at each overdensity Δ in our analysis. The *solid line* shows the number of clusters where the outer radius, R_{out} , to which the quantities in exam are observed is larger than (or equal to) r_{Δ} at the 95 per cent level of confidence [i.e. $R_{\text{out}} \geq (r_{\Delta} - 1.96\sigma)$, where σ is the error quoted in Table 2] as function of the overdensity Δ . The *dotted line* indicates the total number of clusters in our sample. The *dashed line* shows the number of objects that do not satisfy the selection criterion in mass (i.e. $M_{\text{tot}} > 0$ at any given r_{Δ} at the 95 per cent level of confidence; see Sect. 5). The number of objects considered at each Δ is given, therefore, from (*dotted line* – *dashed line*).

1987), with a flat core in the inner part and a r^{-3} dependence at $r \rightarrow \infty$; (ii) the function discussed in Navarro, Frenk & White (1997, hereafter NFW), with a r^{-1} and a $\sim r^{-2.4}$ dependence in the inner and outer parts, respectively:

$$M_{\text{tot,model}}(<r) = 4\pi r_s^3 \rho_s f(x),$$

$$\rho_s = \rho_c \frac{200}{3} \frac{c^3}{\ln(1+c) - c/(1+c)} \quad (4)$$

$$f(x) = \begin{cases} \ln(x + \sqrt{1+x^2}) - \frac{x}{\sqrt{1+x^2}} & \text{(King)} \\ \ln(1+x) - \frac{x}{1+x} & \text{(NFW)} \end{cases}$$

where $x = r/r_s$, ρ_c is the critical density and the relation $r_{\Delta=200} = c \times r_s$ holds for the NFW profile.

Both of these mass models have two free parameters, the core (King) or scale (NFW) r_s and the normalization, that we quote through the concentration parameter c (note that we do this also for a King profile for convenience). For each mass model, we obtain the best-fit values of the two parameters minimizing the χ^2 of the comparison between the deprojected temperature profile and the one obtained from eqn. 3 in two successive steps. First, a minimum in a χ^2 distribution is searched

Table 1. Sample of 22 galaxy clusters considered in this study (see DGM02 for details on the reduction and spectral analysis of the *BeppoSAX* observations). The ‘CF’ column indicates if a cluster is or not a cooling-flow system according to the amount of deposition rate quoted in Peres et al. (1998). R_{out} is the value of the radius at the outer end of the last radial bin considered. The best-fit parameters r_s (in kpc) and c for a King and a NFW dark matter density profile are quoted with the respective errors (in parentheses). Note that A1367 and A3376 do not converge in the $r_s - c$ plane.

Cluster	z	CF	R_{out} kpc/’	King			NFW		
				r_s	c	χ^2 (d.o.f.)	r_s	c	χ^2 (d.o.f.)
A85	0.0518	y	1323/ 16	320 (31)	6.74 (0.36)	4.7 (4)	1282 (133)	2.54 (0.23)	4.3 (4)
A119	0.0440	n	1139/ 16	584 (118)	4.63 (0.48)	7.6 (4)	1097 (48)	2.66 (0.14)	12.9 (4)
A426 (Perseus)	0.0183	y	618/ 20	102 (1)	14.55 (0.13)	55.9 (5)	392 (30)	6.08 (0.27)	25.4 (5)
A496	0.0320	y	845/ 16	203 (14)	8.25 (0.30)	6.0 (4)	738 (66)	3.37 (0.20)	7.4 (4)
A754	0.0528	n	1683/ 20	471 (91)	5.56 (0.61)	25.7 (5)	1619 (104)	2.15 (0.13)	18.3 (5)
A1367	0.0215	n	723/ 20	718 (–)	3.69 (–)	... (5)	718 (–)	2.68 (–)	... (5)
A1656 (Coma)	0.0232	n	777/ 20	184 (48)	10.06 (1.81)	4.2 (5)	459 (242)	5.42 (2.01)	5.1 (5)
A1795	0.0632	y	1584/ 16	314 (22)	6.78 (0.28)	1.5 (4)	1024 (218)	2.93 (0.35)	1.1 (4)
A2029	0.0767	y	1410/ 12	427 (44)	6.14 (0.31)	9.5 (3)	1390 (127)	2.61 (0.20)	6.8 (3)
A2142	0.0899	y	2157/ 16	477 (40)	5.37 (0.26)	2.6 (4)	1654 (285)	2.16 (0.24)	3.6 (4)
A2199	0.0309	y	1022/ 20	175 (11)	9.48 (0.35)	3.7 (5)	560 (157)	4.29 (0.69)	4.0 (5)
A2256	0.0581	n	1469/ 16	570 (68)	4.57 (0.26)	5.3 (4)	1422 (15)	2.19 (0.04)	20.0 (4)
A2319	0.0564	n	1430/ 16	269 (101)	7.65 (1.76)	4.9 (4)	1301 (300)	2.57 (0.68)	3.9 (4)
A3266	0.0594	n	1873/ 20	362 (74)	6.28 (0.86)	2.2 (5)	1576 (182)	2.17 (0.21)	1.9 (5)
A3376	0.0456	n	883/ 12	105 (–)	9.26 (–)	... (3)	176 (–)	6.78 (–)	... (3)
A3526 (Centaurus)	0.0104	y	356/ 20	76 (7)	15.47 (0.67)	3.3 (5)	345 (48)	5.82 (0.60)	3.4 (5)
A3562	0.0483	y	1241/ 16	197 (51)	8.23 (1.49)	5.8 (4)	340 (187)	5.74 (2.50)	6.8 (4)
A3571	0.0391	y	1275/ 20	279 (30)	8.11 (0.48)	7.6 (5)	1122 (192)	3.08 (0.40)	6.2 (5)
A3627	0.0157	n	533/ 20	188 (111)	8.85 (2.55)	18.9 (5)	517 (139)	4.39 (1.57)	19.4 (5)
2A0335	0.0349	y	917/ 16	186 (12)	8.29 (0.28)	6.5 (4)	626 (143)	3.61 (0.52)	7.6 (4)
PKS0745	0.1028	y	1812/ 12	400 (54)	6.04 (0.42)	5.6 (3)	1148 (174)	2.87 (0.40)	5.5 (3)
TRIANG	0.0510	n	1631/ 20	259 (39)	8.61 (0.93)	4.1 (5)	666 (255)	4.47 (1.31)	3.7 (5)

varying these parameters within the following ranges: $10 \text{ kpc} < r_s < \max(2000 \text{ kpc}, R_{\text{out}})$, $1 < c < 15$. This search provides the best-fit values r'_s, c' . A second fit is, then, performed in the restricted ranges: $[\min(r'_s - 300 \text{ kpc}, 10 \text{ kpc}), \max(r'_s + 300 \text{ kpc}, R_{\text{out}})]$, $[\min(c' - 3.0, 0.5), c' + 3.0]$. The results of this refined fit on the scale radius r_s and the concentration parameter c are presented in Table 1. Hereafter, $M_{\text{tot}}(< r)$ is defined for each cluster according to the minimum χ^2 provided from the two mass models considered, $M_{\text{tot,King}}(< r)$ and $M_{\text{tot,NFW}}(< r)$. The error related to the mass estimate is obtained from half the difference between the maximum and the minimum value calculated at each radius for the set of parameters acceptable at 1σ .

From our final sample, we exclude A1367 and A3376 because we do not obtain any χ^2 solution for them. Out of the remaining 20 objects (12 CF and 8 NCF systems), ten (6 of which are CF clusters) are fitted better with a King profile.

We investigate the relations among different physical quantities considering their values at a given overdensity, Δ . This is defined with respect to the critical density, $\rho_{c,z} = (3H_z^2)/(8\pi G)$, and within a cluster described as a sphere with radius r_Δ :

$$\Delta = \frac{3M_{\text{tot}}(< r_\Delta)}{4\pi\rho_{c,z}r_\Delta^3}, \quad (5)$$

with the Hubble constant at redshift z equal to

$$H_z = H_0 \sqrt{\Omega_m(1+z)^3 + 1 - \Omega_m} \quad (6)$$

(for $\Omega_m + \Omega_\Lambda = 1$; i.e., $H_0 \times (1+z)^{3/2}$ for an Einstein–de Sitter universe).

The following analysis has been performed at different overdensities. To handle the observed profiles at any radius, we interpolate linearly all the quantities on scales of 1 kpc. In Fig. 1, we show the number of clusters for which the region enclosing a given overdensity Δ is directly accessible to our X-ray observations. From this figure, we conclude that, at $\Delta = 2500$, 18 galaxy clusters have a detectable X-ray emission and two (A426 and A3526) need an extrapolation of the physical quantities ($R_\Delta/R_{\text{out}} = 1.19$ and 1.34 for A426 and A3526, respectively). As reference value for our results (cf. Table 2), we consider also $\Delta = 1000$, where 11 objects are observable, eight (A85, A119, A426, A496, A1656, A2029, A3526, A3571) need an extrapolation in radius by about 40 per cent (5, 29, 87, 15, 39, 11, 95 and 20 per cent, respectively) and one (A3627) did not satisfy our selection criterion in mass ($\sigma_M/M = 0.62 > 0.51$, see Sect. 5). Furthermore, to compare our results with previous work, we estimate the quantities examined, i.e. gas density, temperature and luminosity, at lower overdensity. For those clusters without observed values at these r_Δ , we extrapolate the interesting quantities using a least squares error-weighted fit with a first-order polyno-

Table 2. Results from the deprojection analysis. All the quantities are estimated within R_Δ (apart from T , which is estimated at R_Δ), where the given overdensity Δ is obtained assuming either a King or NFW functional form for the total mass profile (1σ error in parentheses).

Cluster	R_Δ kpc	$T(R_\Delta)$ keV	T_{ew} keV	T_{mw} keV	L_{bol} $10^{44} \text{ erg s}^{-1}$	M_{gas} $10^{13} M_\odot$	M_{tot} $10^{14} M_\odot$
$\Delta = 2500$							
A85	795 (14)	5.81 (0.79)	6.20 (0.26)	6.28 (0.41)	16.50 (0.45)	5.32 (0.17)	4.25 (0.22)
A119	840 (24)	5.04 (0.69)	6.24 (0.64)	5.90 (0.62)	3.97 (0.27)	2.72 (0.29)	4.90 (0.42)
A426	736 (11)	7.23 (0.26)	5.96 (0.09)	6.94 (0.15)	26.80 (0.28)	4.67 (0.04)	3.06 (0.13)
A496	634 (16)	3.86 (0.31)	4.04 (0.12)	4.14 (0.18)	5.67 (0.16)	2.27 (0.04)	2.04 (0.15)
A754	805 (15)	9.66 (1.51)	9.84 (0.75)	9.89 (0.93)	14.41 (0.53)	5.64 (0.04)	4.42 (0.25)
A1656	720 (42)	8.80 (0.98)	9.65 (0.85)	9.40 (0.84)	14.04 (0.75)	4.68 (0.07)	2.91 (0.51)
A1795	771 (12)	5.62 (0.73)	5.82 (0.14)	5.92 (0.30)	21.91 (0.36)	5.37 (0.07)	4.00 (0.19)
A2029	895 (16)	8.79 (1.00)	7.83 (0.29)	8.50 (0.50)	41.33 (0.98)	8.13 (0.16)	6.50 (0.34)
A2142	862 (12)	8.66 (0.81)	8.66 (0.26)	8.90 (0.38)	48.59 (0.97)	9.92 (0.08)	6.02 (0.25)
A2199	642 (12)	4.77 (0.85)	4.46 (0.16)	4.64 (0.34)	6.73 (0.19)	2.34 (0.09)	2.10 (0.12)
A2256	802 (12)	6.41 (0.49)	7.17 (0.24)	6.91 (0.27)	14.56 (0.38)	5.93 (0.09)	4.44 (0.19)
A2319	821 (36)	10.20 (2.64)	9.78 (0.90)	9.94 (1.30)	28.00 (1.33)	7.67 (0.15)	4.74 (0.63)
A3266	792 (20)	9.08 (1.34)	9.38 (0.67)	9.33 (0.78)	14.46 (0.77)	4.72 (0.13)	4.29 (0.32)
A3526	476 (20)	2.66 (0.19)	3.43 (0.14)	3.37 (0.16)	1.73 (0.08)	0.84 (0.02)	0.81 (0.10)
A3562	614 (33)	4.86 (1.40)	5.46 (0.59)	5.28 (0.80)	3.35 (0.31)	1.79 (0.16)	1.94 (0.31)
A3571	900 (21)	6.04 (0.61)	7.40 (0.33)	7.01 (0.39)	15.97 (0.48)	5.87 (0.15)	5.95 (0.42)
A3627	639 (98)	5.39 (1.06)	6.08 (0.98)	5.96 (0.96)	4.31 (0.59)	1.99 (0.12)	1.98 (0.91)
2A0335	583 (11)	2.94 (0.30)	3.00 (0.07)	3.13 (0.15)	7.06 (0.18)	1.98 (0.10)	1.60 (0.09)
PKS0745	841 (13)	8.75 (1.14)	7.43 (0.17)	8.19 (0.43)	60.67 (0.80)	8.95 (0.07)	5.79 (0.26)
TRIANG	859 (23)	9.39 (1.34)	10.21 (0.52)	9.92 (0.69)	29.72 (0.97)	7.17 (0.17)	5.34 (0.44)
$\Delta = 1000$							
A85	1393 (31)	4.05 (0.43)	6.01 (0.24)	5.40 (0.30)	19.37 (0.49)	11.33 (0.25)	9.14 (0.61)
A119	1467 (88)	2.17 (0.30)	5.25 (0.54)	4.07 (0.43)	6.61 (0.50)	6.97 (0.67)	10.44 (1.88)
A426	1156 (22)	7.48 (0.27)	6.54 (0.10)	7.61 (0.16)	37.61 (0.39)	9.09 (0.07)	4.74 (0.27)
A496	968 (29)	3.31 (0.26)	3.99 (0.12)	3.88 (0.17)	6.54 (0.19)	4.24 (0.08)	2.90 (0.26)
A754	1449 (27)	7.17 (0.86)	9.39 (0.63)	8.73 (0.66)	23.96 (0.82)	15.23 (0.17)	10.32 (0.57)
A1656	1078 (80)	7.90 (0.88)	9.30 (0.82)	8.91 (0.80)	22.20 (1.19)	10.61 (0.16)	3.90 (0.87)
A1795	1321 (36)	3.69 (0.44)	5.73 (0.14)	5.15 (0.25)	23.91 (0.44)	10.11 (0.19)	8.05 (0.65)
A2029	1561 (32)	5.04 (0.57)	7.67 (0.28)	7.12 (0.42)	46.63 (1.12)	17.91 (0.27)	13.80 (0.86)
A2142	1426 (35)	6.85 (0.72)	8.49 (0.26)	8.03 (0.38)	58.18 (1.26)	19.89 (0.38)	10.90 (0.80)
A2199	966 (22)	3.85 (0.39)	4.43 (0.12)	4.41 (0.21)	7.46 (0.18)	4.09 (0.13)	2.87 (0.19)
A2256	1410 (46)	3.91 (0.32)	6.76 (0.33)	5.71 (0.30)	19.12 (0.72)	13.50 (0.22)	9.65 (0.95)
A2319	1437 (86)	11.39 (1.96)	10.08 (0.91)	10.60 (1.16)	38.44 (1.87)	17.89 (0.32)	10.16 (1.83)
A3266	1424 (44)	6.66 (1.22)	8.96 (0.73)	8.21 (0.79)	20.62 (1.14)	13.01 (0.51)	9.98 (0.93)
A3526	694 (31)	2.13 (0.15)	3.41 (0.14)	3.11 (0.15)	2.67 (0.12)	1.78 (0.05)	1.00 (0.13)
A3562	937 (67)	3.22 (0.72)	4.94 (0.49)	4.20 (0.56)	4.24 (0.39)	3.86 (0.36)	2.76 (0.59)
A3571	1532 (53)	2.24 (0.23)	6.94 (0.31)	5.20 (0.29)	19.10 (0.53)	13.18 (0.23)	11.73 (1.21)
A3627	968 (199)	4.74 (0.94)	5.59 (0.90)	5.46 (0.88)	10.29 (1.42)	4.77 (0.29)	2.76 (1.70)
2A0335	890 (22)	2.02 (0.20)	2.96 (0.07)	2.73 (0.13)	7.61 (0.18)	3.47 (0.10)	2.27 (0.16)
PKS0745	1446 (36)	9.08 (1.22)	7.51 (0.18)	8.53 (0.48)	65.11 (0.92)	15.81 (0.21)	11.78 (0.88)
TRIANG	1392 (67)	6.67 (0.85)	9.78 (0.62)	8.69 (0.66)	36.81 (1.45)	15.17 (0.49)	9.10 (1.32)

mial performed with the `svdfit` function (Press et al. 1992, sect. 15.4) on the logarithmic values of the variables observed in the outer region where $r > 0.7 \times R_{\text{out}}$. The mean relative error measured in the observed region is propagated to the extrapolated values.

For a given overdensity Δ , we quote in Table 2 the values of $M_{\text{tot}}(< r_\Delta)$, r_Δ , several estimates of the gas temperature (see Sect. 5), $L_{\text{bol}}(< r_\Delta)$ and $M_{\text{gas}}(< r_\Delta)$.

4.1. X-ray mass: comparison with $\beta\gamma$ -model

In this section, we compare the estimates of the dark matter profile we have obtained in the previous subsection with results derived from modelling the gas density profile and applying (i) the hydrostatic equilibrium and (ii) a polytropic shape of the temperature profile. The latter procedure is generally applied in the X-ray analysis of galaxy clusters and makes use of the β -model, $\rho_{\text{gas}} \propto (1 + x^2)^{-1.5\beta}$ (Cavaliere & Fusco-Femiano

1976), to reproduce the observed surface brightness profile (an analytic expression can be obtained if T_{gas} is assumed constant; for a generalization to the polytropic case see Ettori 2000) and build a temperature profile as function of the polytropic index γ like $T_{\text{gas}} \propto (1+x^2)^{-1.5\beta(\gamma-1)}$.

In the $\beta\gamma$ -model the total mass profile is readily derived from eqn. 3

$$\begin{aligned} \frac{M_{\text{tot},\beta\gamma}(<r)}{10^{14}h_{50}^{-1}M_{\odot}} &= 1.11 \frac{0.6}{\mu} \beta \gamma T(r) r_c \frac{x^3}{(1+x^2)} \\ &= 1.11 \frac{0.6}{\mu} \beta \gamma T_0 r_c \frac{x^3}{(1+x^2)^{1.5\beta(\gamma-1)+1}} \end{aligned} \quad (7)$$

This formula has been applied to estimate the total mass profile in recent work that considered a measured temperature profile from *ASCA* data (e.g. Markevitch et al. 1999 on A496 and A2199; Nevalainen, Markevitch & Forman 2000, Finoguenov, Reiprich & Böhringer 2001).

In fig. 2, we compare our mass profiles (from the King functional form, cf. Table 1) for two CF clusters (A496 and A2199) with those derived by Markevitch et al. (1999) using the $\beta\gamma$ model. The larger deviations ($|\sigma_M| > 3\sigma$) are localized in the region $\sim 100 - 500$ kpc (and below 100 kpc and above 1 Mpc in A496) and introduce a systematic error that could contribute to the observed scatter in the distribution of the measurements. It is worth noticing that the polytropic temperature profile does not reproduce in a satisfactory way the temperature profile of either A496 or A2199, as can be seen in fig. 2. DGM02 have shown that the temperature profiles of our *BeppoSAX* sample of clusters are in general not in good agreement with polytropic temperature profile. This discrepancy should be taken into consideration when applying the $\beta\gamma$ model to derive mass measurements of galaxy clusters.

4.2. X-ray mass: comparison with optical estimates

Girardi et al. (1998) quote the optically-determined mass estimates for 15 out of 20 of our clusters (not available for A3526, A3627, 2A0335, PKS0745, TRIANG). In Fig. 3, we show a comparison between X-ray measurements at $\Delta = 1000$ and the optical masses estimated at the same r_{Δ} by using the Jeans equation ($M_{\text{iso}} = 3\beta_{\text{gal}}\sigma_p^2 r/G$, where β_{gal} is the exponent in the King-like galaxy density profile and σ_p is the projected velocity dispersion). This mass estimate is consistent with the corrected virial mass as discussed in Girardi et al. (1998, Section 5). Moreover, by making use of the relation $\sigma^2 = (GM_{200})/(2r_{200})$ between the velocity dispersion in the dark matter distribution and the total mass within r_{200} , we derive $\sigma_X = \sqrt{50} H_0 r_{200} = \sqrt{50} H_0 c r_s$ for a NFW potential and compare our estimates of σ_X from the best-fit values in Table 1 to the optically-determined velocity dispersion, σ_p .

Out of 16 clusters examined, we observe two systems (A119 and A754) lying with a relative difference in mass larger than 3σ . When the optically and X-ray determined velocity dispersions are compared, three objects (A119, A754 and A2256) show significant deviations (see Fig. 3). These three clusters are NCF systems, are known to have irregular and

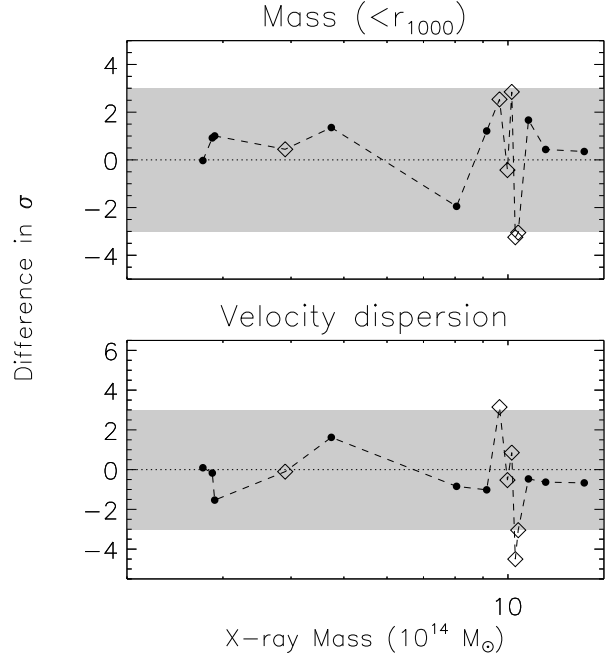


Fig. 3. Differences (in σ) between the interpolated optical values and the measured X-ray mass and velocity dispersion versus the measured X-ray mass (see text for details). *Filled circles* represent CF galaxy clusters, whereas *open squares* are NCF objects.

asymmetric X-ray brightness and, at least for A754 and A2256, are indeed involved in massive merging (e.g., A119: Ferretti et al. 1999; A754: Henriksen & Markevitch 1996; A2256: Molendi, De Grandi & Fusco-Femiano 2000) that may affect both the optical determinations of the velocity dispersion and the validity of the hydrostatic assumption made in the process of the estimation of the X-ray mass.

In general, we measure a median deviation of about 1.2 and 0.8 σ in mass and velocity dispersion measurements, respectively. Moreover, there is evidence that larger deviations are present in the subsample of NCF, not-relaxed systems (2.7 and 2.0 σ deviation in mass and velocity dispersion, respectively, for NCF; 1.0 and 0.7 σ for CF).

5. Relations among the observed quantities

Our refined sample of 20 nearby ($0.010 < z < 0.103$; median redshift of 0.050) clusters of galaxies spans a factor of more than three in mass-weighted temperature ($3.1 \text{ keV} < T_X < 9.9 \text{ keV}$; median value: 6.9 keV) and two orders of magnitude in luminosity ($1.7 \times 10^{44} \text{ erg s}^{-1} < L_X < 6.1 \times 10^{45} \text{ erg s}^{-1}$; median value: $1.5 \times 10^{45} \text{ erg s}^{-1}$). In the following analysis, we consider only the clusters with a total mass at a given radius larger than zero at the 95 per cent level of confidence, i.e. we select just the objects with $\sigma_M/M < (1/1.96) = 0.51$.

In the present work, we investigate the correlations between the observed physical quantities in order to assess the robustness of the self-similar scaling relations for clusters of galaxies

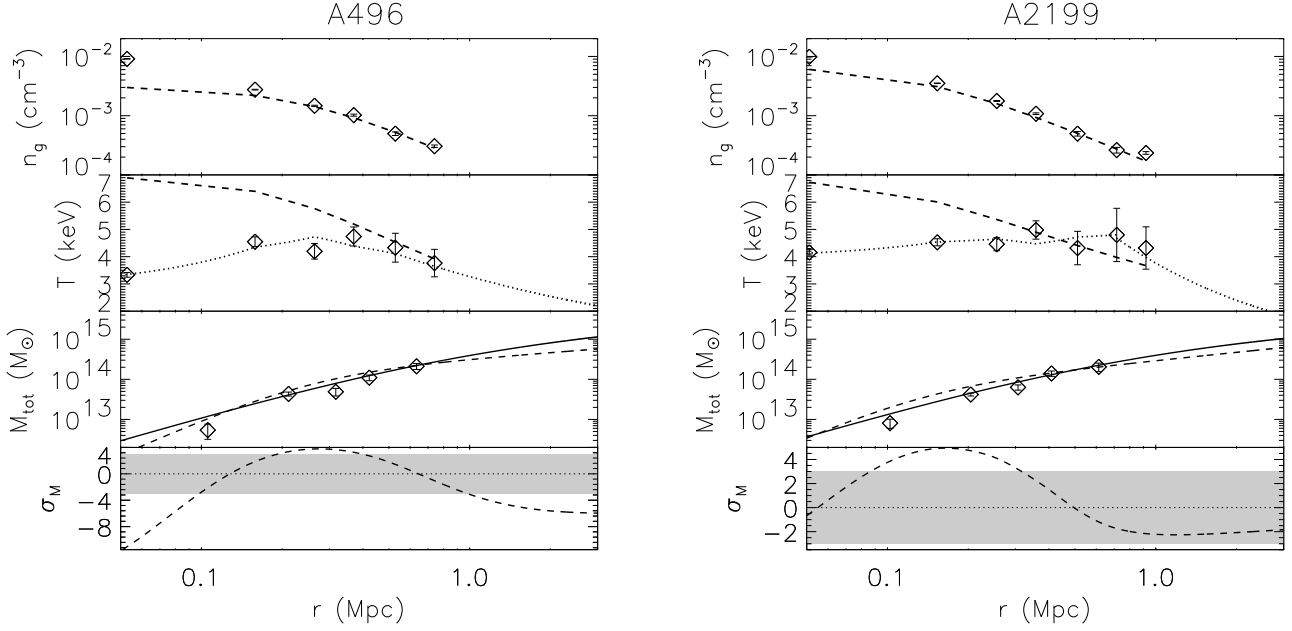


Fig. 2. Comparison between deprojected (diamonds) observed values and best-fit $\beta\gamma$ -model (dashed line) for gas density, temperature and total gravitating mass. The dotted line indicates the best-fit temperature profile for a given mass model as described in Sect. 4.

(e.g. Kaiser 1986). These relations are the product of simple assumptions on the formation and evolution of galaxy clusters. As non-linear structures, they are assumed to form by homogeneous spherical collapse of gravitational instabilities of dark matter on which gas infalls are heated up by shocking processes. If no dissipation is considered, adiabatic X-ray emitting plasma can be considered to share the same potential well with dark matter with a spatial distribution that can be different from the dark matter's one but has to be the same at any earlier epoch (e.g. Bryan & Norman 1998, Arnaud & Evrard 1999). However, deviations are expected from self-similarity under the effects of, for example, the dynamical history of clusters as three-dimensional aggregation of clumps (Jing & Suto 2000, Thomas et al. 2001) and any additional physics acting on the intracluster gas over the simplistic infall in the potential well (e.g. Evrard & Henry 1991; David, Forman & Jones 1991; Bryan & Norman 1998; Bialek, Evrard & Mohr 2001; Borgani et al. 2002 and references therein). The latter case is particularly relevant to cool systems where the extra energetic amount required from their observed properties is comparable to their thermal energy (e.g. Ponman et al. 1996; Ponman, Cannon & Navarro 1999; Tozzi & Norman 2001). Our sample encloses only clusters with temperature larger than about 3 keV and, thus, is expected not to be affected in a significant way by any increase of the gas entropy occurring during the cluster formation history. Therefore, we are able to investigate the galaxy cluster scaling laws excluding systematics related to the energetic budget.

Table 3. Spearman's ρ rank correlation results on a set of physical quantities. A small value in probability indicates significant correlation. $n\sigma$ indicates the number of standard deviations by which the dependence in exam deviates from the null-hypothesis of uncorrelated data sets. The gas-mass-weighted temperature, T_{mw} , is here used.

relation	ρ	$\Delta = 2500$		$\Delta = 1000$		
		Prob	$ n\sigma $	Prob	$ n\sigma $	
$M_{\Delta} - T_{\Delta}$	0.69	0.001	3.00	0.54	0.017	2.29
$R_{\Delta} - T_{\Delta}$	0.71	<0.001	3.09	0.54	0.017	2.29
$L_{\Delta} - T_{\Delta}$	0.65	0.002	2.83	0.74	<0.001	3.16
$M_{\text{gas},\Delta} - T_{\Delta}$	0.77	<0.001	3.34	0.79	<0.001	3.35
$f_{\text{gas},\Delta} - T_{\Delta}$	0.58	0.007	2.52	0.31	0.204	1.30
$L_{\Delta} - M_{\Delta}$	0.75	<0.001	3.26	0.64	0.003	2.70

In our analysis, we adopt three different definitions for the plasma temperature at a given overdensity Δ :

1. the gas temperature in the shell at r_{Δ} ,

$$T(r_{\Delta}) = T_i(r_{\Delta}), \quad (8)$$

2. the emission-weighted gas temperature *within* r_{Δ} ,

$$T_{\text{ew}}(< r_{\Delta}) = \frac{\sum_i^{0 < r_i < r_{\Delta}} L_i T_i}{\sum_i^{0 < r_i < r_{\Delta}} L_i} = \frac{\sum_i^{0 < r_i < r_{\Delta}} L_i T_i}{L(< r_{\Delta})}, \quad (9)$$

3. the mass-weighted gas temperature *within* r_Δ ,

$$T_{\text{mw}}(< r_\Delta) = \frac{\sum_i^{0 < r_i < r_\Delta} M_{\text{gas},i} T_i}{\sum_i^{0 < r_i < r_\Delta} M_{\text{gas},i}} = \frac{\sum_i^{0 < r_i < r_\Delta} M_{\text{gas},i} T_i}{M_{\text{gas}}(< r_\Delta)}, \quad (10)$$

where i indicates the running cursor on shells and j on rings. We use the values of the temperature in the volume shells obtained from the best-fit procedure discussed in Sect. 4. In Fig. 4, we show the temperature profiles defined above for a typical CF (A496) and NCF (A754) galaxy cluster.

To check for the presence of linear dependence between the logarithmic values of the physical quantities being studied, we have performed both a non-parametric and a parametric analysis of our data. The two approaches can be considered as complementary: the non-parametric analysis has the advantage of not relying on a specific model but does not treat errors; the parametric analysis, which assumes a power-law model, provides a treatment for errors.

For the non-parametric analysis we have used the Spearman's ρ rank correlation of two sample populations (Press et al. 1992, p.634). We quote in Table 3 the set of pair quantities with the respective Spearman's ρ and probability. Relations with a $\sim 3\sigma$ deviation from the null hypothesis of uncorrelated datasets are present amongst the gravitating mass, the gas temperature, the gas luminosity and the gas mass. A weaker dependence appears between the gas mass fraction and the temperature.

In our parametric analysis, we use the bisector modification (i.e. the best-fit results bisect those obtained from minimization in vertical and horizontal directions) of the linear regression algorithm in Akritas & Bershady (1996 and references therein, hereafter BCES) that takes into account both any intrinsic scatter and errors on the two variables considered as symmetric. The uncertainties on the best-fit results are obtained from 10,000 bootstrap resamplings.

5.1. $M_{\text{tot}} - T$ relation

In this and the following subsections we shall compare the the normalization and slope of the scaling relations obtained from our data to theoretical predictions based on the simplistic assumption of an isothermal sphere for both the gas represented by its temperature and the collisionless dark matter particles (e.g. Kaiser 1986, Bryan & Norman 1998). As usual we indicate with $\beta_T = (\mu m_p \sigma^2)/(kT_{\text{gas}})$, the ratio between the energy in the plasma and in the dark matter with velocity dispersion, σ . An isothermal distribution function is characterized by a proportional relation between the matter density and the velocity dispersion, $\rho(r) \propto \sigma^2/r^2$ (Binney & Tremaine 1987). This implies a total mass within a radius r of $(2\beta_T kT)/(G\mu m_p) r$ that can be compared to eqn. 5 to infer the relation between M_{tot} and T_{gas} at given overdensity Δ :

$$\frac{M_{\text{tot}}(< r_\Delta)}{10^{14} h_{50}^{-1} M_\odot} = 0.38 \beta_T^{3/2} \left(\frac{50}{H_z}\right) \left(\frac{1000}{\Delta}\right)^{1/2} \left(\frac{T_{\text{gas}}}{\text{keV}}\right)^{3/2},$$

$$\log M_{14} = -0.42 + 1.5 \log T \left(+ \log \left(\beta_T^{3/2} f_\Omega \right) \right), \quad (11)$$

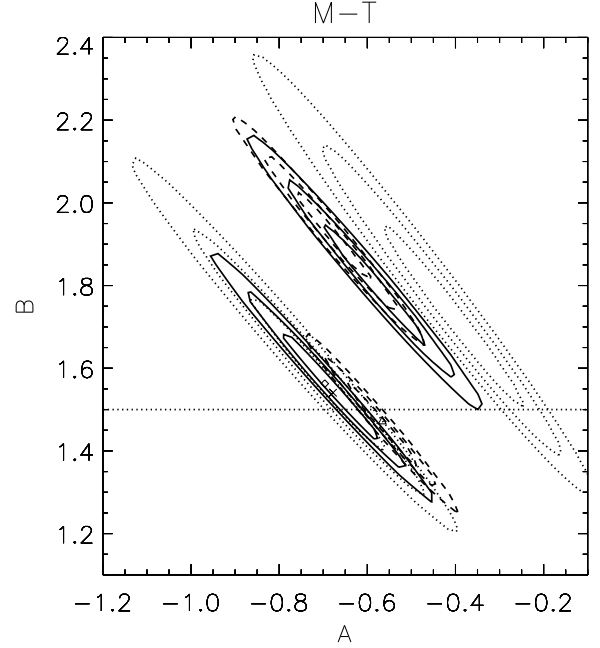


Fig. 6. Plot of 1, 2, 3 σ contour from χ^2 statistic for the two interesting parameters of the linear fit applied to $M - T_{\text{mw}}$ (solid line), $M - T_{\text{ew}}$ (dashed line), $M - T(R)$ (dotted line) relations at $\Delta = 2500$ and 1000 (the latter ones have higher normalization A).

where H_z is the Hubble constant at redshift z given in eqn. 6, $f_\Omega \equiv \left(\frac{50}{H_z}\right) \left(\frac{1000}{\Delta}\right)^{1/2}$ and in the bottom row we have rewritten the relation in log-log form. The assumption on the dark matter profile only affects the value of the normalization. We consider the isothermal case here adopted as a reference.

In the considerations above, we have adopted the assumption that we are observing clusters just after their virialization (cfr. Voit & Donahue 1998 for the implication on the $M - T$ relation of clusters that gradually form and stop evolving in a low density Universe). The $M - T$ relation makes reasonable assumptions that have been tested both in numerical simulations and in observations. Moreover, this is a direct result coming from the combination of the conservation of energy throughout nearly-spherical collapse of clusters with the virial theorem (Afshordi & Cen 2002).

In Table 4 and Fig. 5, we show the results of the fitting analysis. A segregation is noticeable between CF and NCF objects. When we fit the twelve CF clusters, we measure $M_{14} = 0.12(\pm 0.06) \times T_{\text{mw}}^{1.88(\pm 0.27)}$. When only the 8 NCF systems are considered, $M_{14} = 0.92(\pm 2.01) \times T_{\text{mw}}^{0.73(\pm 1.00)}$. The slope does not show any significant change at the variation of the overdensity at which the quantities examined are considered (see Fig. 7).

We compare now these results on the normalization and slope of the $M - T$ relation with the values obtained in previous work.

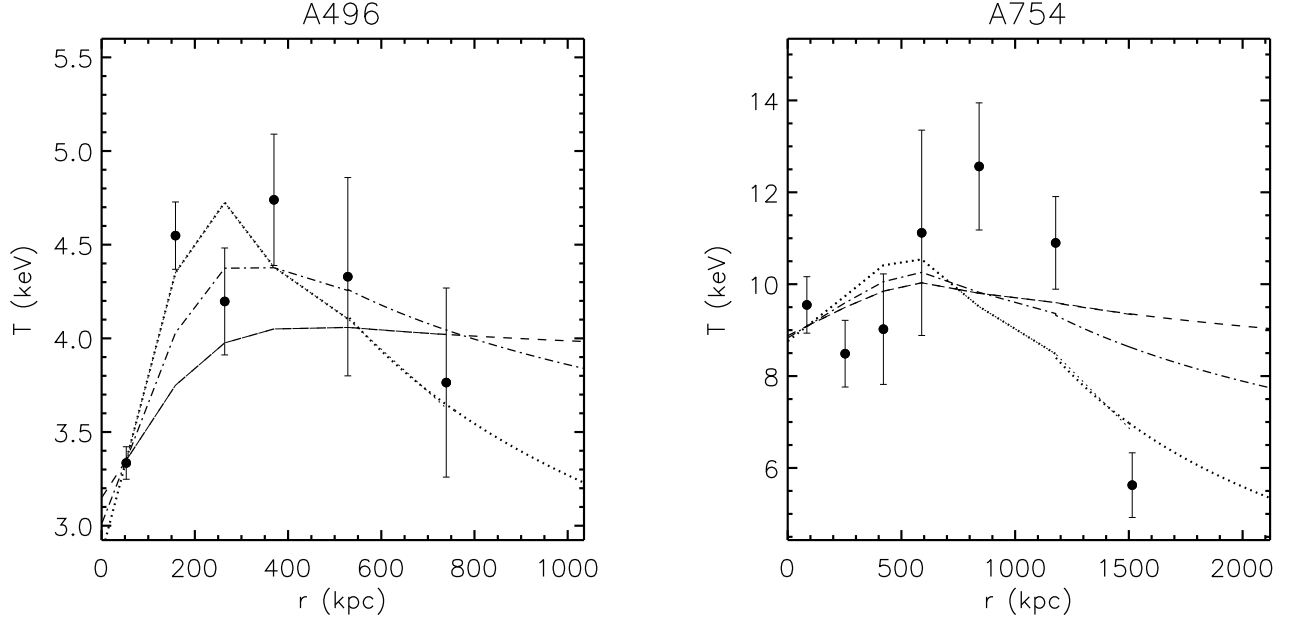


Fig. 4. The temperature defined in eqn. 8, 9 and 10 are here plotted (*dotted*, *dashed* and *dot-dashed*, respectively) with the de-projected data points.

Table 4. Results of the best-fit analysis. When the value of the slope is investigated, we apply the linear BCES bisector estimator to the logarithmic of the power law $Y = aX^b$, $\log Y = A + B \log X$ (i.e. $a = 10^A, b = B$; errors in parentheses). The temperature, T , is in unit of keV; the luminosity, L , in $10^{44} h_{50}^{-2}$ erg s $^{-1}$; the total mass, M , in $10^{14} h_{50}^{-1} M_{\odot}$; the gas mass, M_{gas} , in $10^{13} h_{50}^{-5/2} M_{\odot}$; the radius at given overdensity, R , in $100 h_{50}^{-1}$ kpc; the gas fraction, f_{gas} , in $h_{50}^{-3/2}$. When the slope B is fixed, we estimate the median of the distribution of $\log Y - B \log X$. The scatter on Y is measured as $\left[\sum_{j=1, N} (\log Y_j - A - B \log X_j)^2 / N \right]^{1/2}$. Note that the scatter along the X-axis can be estimated as $\sigma_{\log X} = \sigma_{\log Y} / B$.

relation	$\Delta = 2500$			$\Delta = 1000$		
	A	B	$\sigma_{\log Y}$	A	B	$\sigma_{\log Y}$
$M_{14} - T_{\text{mw}}$	-0.70 (0.18)	1.54 (0.22)	0.14	-0.52 (0.28)	1.76 (0.34)	0.25
	-0.60 (0.15)	1.50 (fix)	0.16	-0.34 (0.20)	1.50 (fix)	0.24
$M_{14} - T_{\text{ew}}$	-0.67 (0.20)	1.51 (0.24)	0.15	-0.73 (0.27)	1.94 (0.32)	0.22
	-0.60 (0.16)	1.50 (fix)	0.16	-0.39 (0.18)	1.50 (fix)	0.20
$M_{14} - T(R)$	-0.61 (0.14)	1.47 (0.18)	0.15	-0.52 (0.32)	1.24 (0.45)	0.31
	-0.64 (0.16)	1.50 (fix)	0.15	-0.24 (0.29)	1.50 (fix)	0.35
$L_{44} - T_{\text{mw}}$	-1.21 (0.47)	2.79 (0.55)	0.31	-0.61 (0.26)	2.37 (0.33)	0.22
	-0.54 (0.32)	2.00 (fix)	0.28	-0.32 (0.24)	2.00 (fix)	0.21
$L_{44} - T_{\text{ew}}$	-1.07 (0.47)	2.64 (0.55)	0.34	-0.82 (0.34)	2.54 (0.42)	0.25
	-0.54 (0.37)	2.00 (fix)	0.31	-0.41 (0.27)	2.00 (fix)	0.23
$L_{44} - T(R)$	-1.09 (0.45)	2.73 (0.54)	0.29	-0.61 (0.20)	1.76 (0.27)	0.27
	-0.47 (0.33)	2.00 (fix)	0.26	-0.13 (0.30)	2.00 (fix)	0.29
$M_{\text{gas},13} - T$	-0.93 (0.25)	1.91 (0.29)	0.16	-0.35 (0.18)	1.74 (0.22)	0.16
	-0.57 (0.18)	1.50 (fix)	0.15	-0.20 (0.17)	1.50 (fix)	0.15
$R_{100} - T$	0.51 (0.05)	0.47 (0.07)	0.04	0.65 (0.10)	0.60 (0.13)	0.08
	0.50 (0.04)	0.50 (fix)	0.05	0.72 (0.06)	0.50 (fix)	0.08
$f_{\text{gas}} - T$	-1.42 (0.27)	0.61 (0.31)	0.11	-1.34 (0.26)	0.66 (0.34)	0.13
	-0.90 (0.10)	0.00 (fix)	0.11	-0.85 (0.08)	0.00 (fix)	0.12
$L_{44} - M_{14}$	0.06 (0.15)	1.84 (0.23)	0.26	0.16 (0.14)	1.28 (0.15)	0.27
	0.31 (0.19)	1.33 (fix)	0.25	0.14 (0.21)	1.33 (fix)	0.27

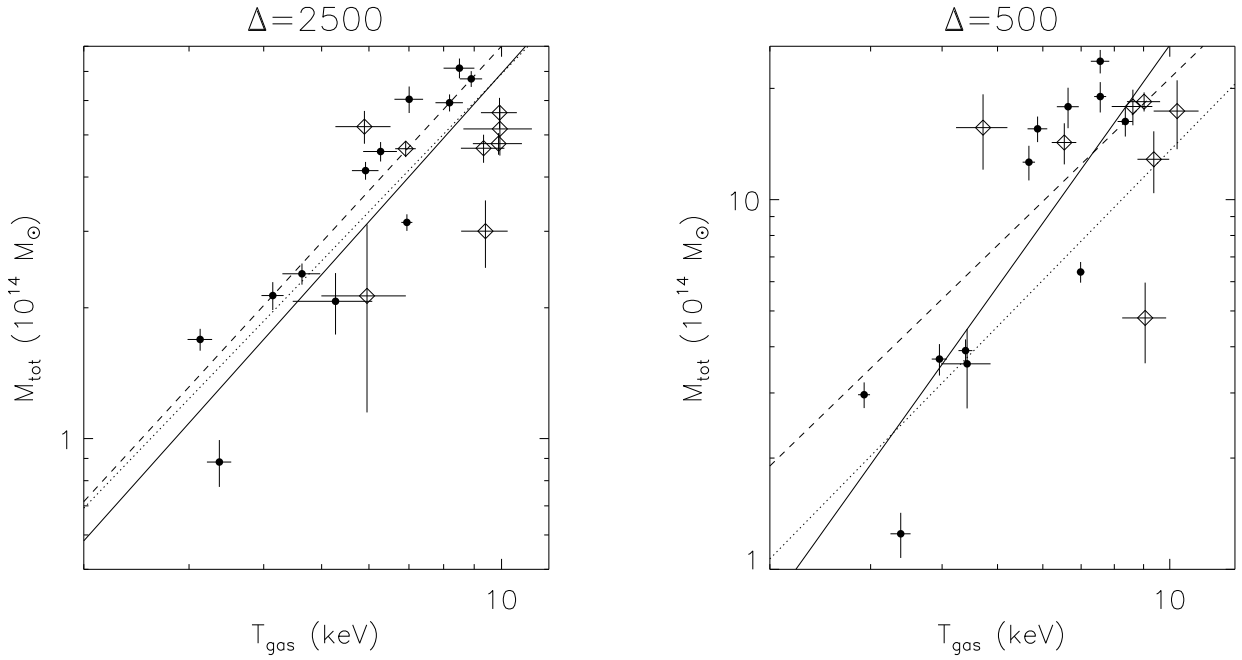


Fig. 5. $M - T_{\text{mw}}$ relation. The *solid* and *dashed* lines represent our best-fit results for the given overdensity, using the slope as free parameter and fixing it to 1.5, respectively. *Filled circles* represent CF galaxy clusters, whereas *open squares* are NCF objects. (Left) The best-fit slope is $1.54(\pm 0.22)$. The *dotted* line represents the best-fit result from Allen et al. (2001; $\Delta = 2500$). (Right) Best-fit of the $M - T_{\text{ew}}$ relation at $\Delta = 500$ (slope: 2.17 ± 0.37). The *dotted* line shows the best-fit from Finoguenov et al. (2001).

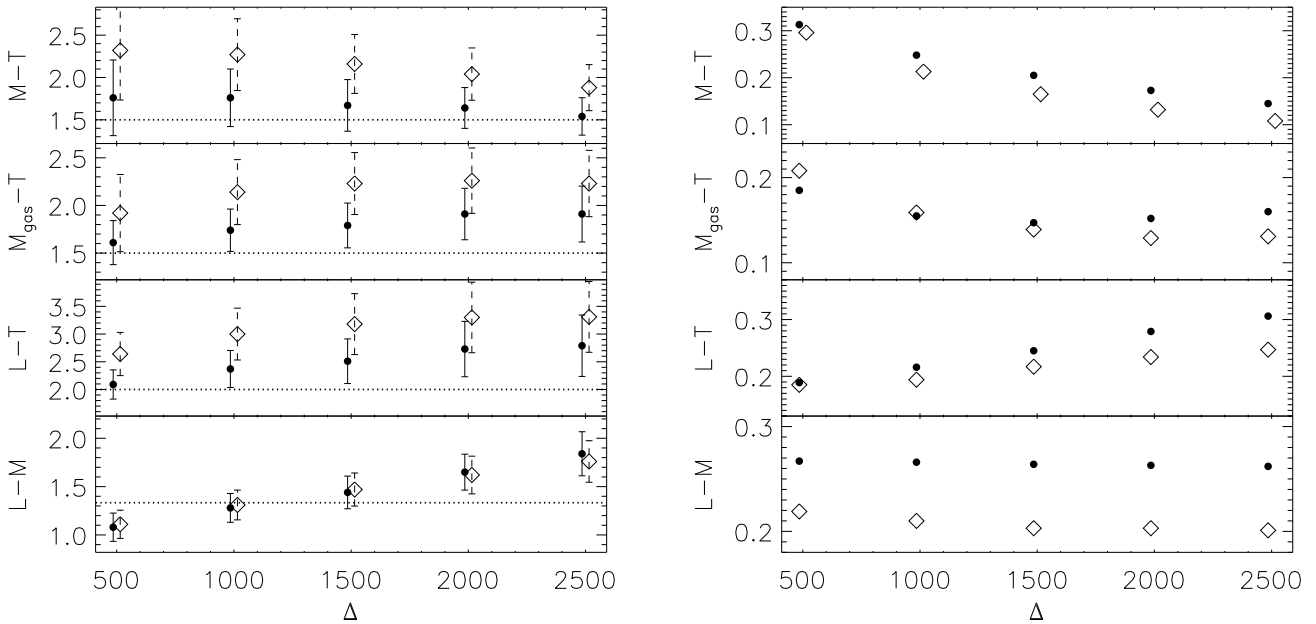


Fig. 7. (Left) Behaviour of the slope in the $M - T_{\text{mw}}$, $M_{\text{gas}} - T_{\text{mw}}$, $L - T_{\text{mw}}$ and $L - M$ relations as function of the considered overdensity. The *diamonds* + dashed error bars show the results for CF systems only. The dotted lines indicate the values predicted from the scaling laws. (Right) Values of the scatter of the same relations. *Full dots* represent the entire sample, whereas the *diamonds* indicate the results for CF objects.

In numerical simulations, fixing the slope to $3/2$, the normalization β_T in eqn. 11 ranges between 1.15 (model *CL2* in Navarro, Frenk & White 1995) to 1.24 (Evrard, Metzler & Navarro 1996) and ~ 1.3 (Bryan & Norman 1998; cfr. their Table 2). We measure a normalization β_T of $1.14(\pm 0.34)$ that is consistent with the results quoted for simulated clusters. For example, we obtain a best-fit correlation of $M_{14} = 0.46(\pm 0.21) \times T_{\text{mw}}^{1.5}$ ($\Delta = 1000$), that has a normalization lower by 13 per cent (and only 0.3σ apart) than the value measured at the same overdensity in the gas-dynamic simulations of Evrard et al. (1996).

From an observational point of view, Horner, Mushotzky & Scharf (1999) claim that the $M - T$ relation is steeper than the traditional scaling, following a $\propto T^{1.8-2.0}$ law, when the mass is estimated according to the β -model. Slopes steeper than virial prediction are also observed in high-redshift clusters (Schindler 1999) and highly-luminous clusters (Ettori & Fabian 1999) samples, where isothermality is assumed. Moreover, Neumann & Arnaud (1999) from a β -model estimate of the gravitating mass obtain a $M - T$ relation consistent with the classical scaling relation. Nevalainen, Markevitch & Forman (2000) from a sample of 6 clusters and 3 groups/galaxies with temperature profiles observed from *ASCA* and *ROSAT*, respectively, inferred at $\Delta = 1000$ a slope of $1.79(\pm 0.09)$ and a normalization significantly lower than the one observed in simulations, suggesting evidence of breaking of the self-similarity in the less massive systems due to heating processes. Finoguenov, Reiprich & Böhringer (2001) studied two samples of clusters, one comprising a complete sample of 63 bright objects from the *ROSAT* All Sky Survey with an assigned emission-weighted temperature collected from the literature and the other including 39 systems (22 of these with $T < 3.5$ keV) with known temperature profiles that are used to infer the total mass in combination with a $\beta\gamma$ -model (see Section 4.1 above). Correlating $M_{\text{tot}}(< r_{500})$ with an emission-weighted temperature, these authors find a slope of $1.58(\pm 0.07)$ for the sample with a resolved temperature profile and excluding objects with $M_{500} < 5 \times 10^{13} M_{\odot}$ (the slope increases slightly to 1.78 ± 0.09 for the whole sample, consistent with the result from the flux limited sample). The normalization is more than 50 per cent lower than the value quoted in Evrard et al. (1996). Allen, Schmidt & Fabian (2001), using spatially resolved X-ray spectroscopy with the *Chandra* observatory of five highly massive cooling-flow (and so, relaxed) galaxy clusters at intermediate redshifts, found consistency with the scaling law prediction and a normalization 40 per cent lower (but with a deviation significant only to 1.8σ considering their quoted values) than what is observed in simulated clusters.

It is worth noticing that a tight correlation between the parameters A and B of the linear fit performed on the logarithmic values appears from the contour plot of the probability distribution obtained applying the χ^2 statistic (see Fig. 6). In this situation, any slope larger than 1.5 (i.e. $B > 1.5$) requires a lower normalization A consistent with what is generally observed.

We show in Fig. 5 a comparison with the recent results from Finoguenov et al. (2001) and Allen et al. (2001). Both are con-

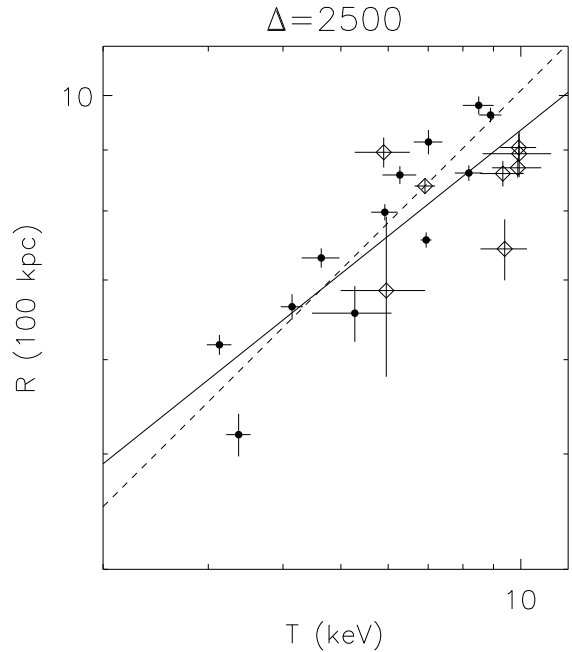


Fig. 8. $R - T_{\text{mw}}$ relation. The solid line represents the best-fit slope of $0.47(\pm 0.07)$; the dashed line is obtained fixing the slope to $1/2$. Filled circles represent CF galaxy clusters, whereas open squares are NCF objects.

sistent with our results. For example, Allen et al. measure a normalization that is 13 per cent lower than ours with a difference of about 0.4σ .

Another way to consider the relation between the gas temperature and a physical quantity related to the overdensity typical of a cluster, is the $R - T$ relation, where R is the radius of a sphere enclosing a given overdensity. It can be obtained directly from eqn. 11

$$\frac{R}{100h_{50}^{-1}\text{kpc}} = 5.07 \beta_T^{1/2} \left(\frac{50}{H_z}\right) \left(\frac{1000}{\Delta}\right)^{1/2} \left(\frac{T}{1\text{keV}}\right)^{1/2},$$

$$\log R_{100} = 0.71 + 0.5 \log T \left(+ \log \left(\beta_T^{1/2} f_{\Omega} \right) \right). \quad (12)$$

Fitting a power law as done above, we obtain $R_{100} = 3.27(\pm 0.41) \times T_{\text{mw}}^{0.47(\pm 0.07)}$ ($\Delta = 2500$; cf. Table 4 and Fig. 8). Fixing the slope to $1/2$ in accordance with what predicted from scaling laws the normalization is of $530(\pm 79)$ kpc ($\Delta = 1000$), only 0.4σ below the value of 566 kpc measured in the hydrodynamics simulations of Evrard et al. (1996).

5.2. $M_{\text{gas}} - T$ relation

The gas mass fraction

$$f_{\text{gas}}(r_{\Delta}) = \frac{M_{\text{gas}}(< r_{\Delta})}{M_{\text{tot}}(< r_{\Delta})}, \quad (13)$$

should be constant in a population of galaxy clusters that satisfies the self-similar behaviour. Once the self-similarity is broken, a dependence of f_{gas} on the temperature is expected

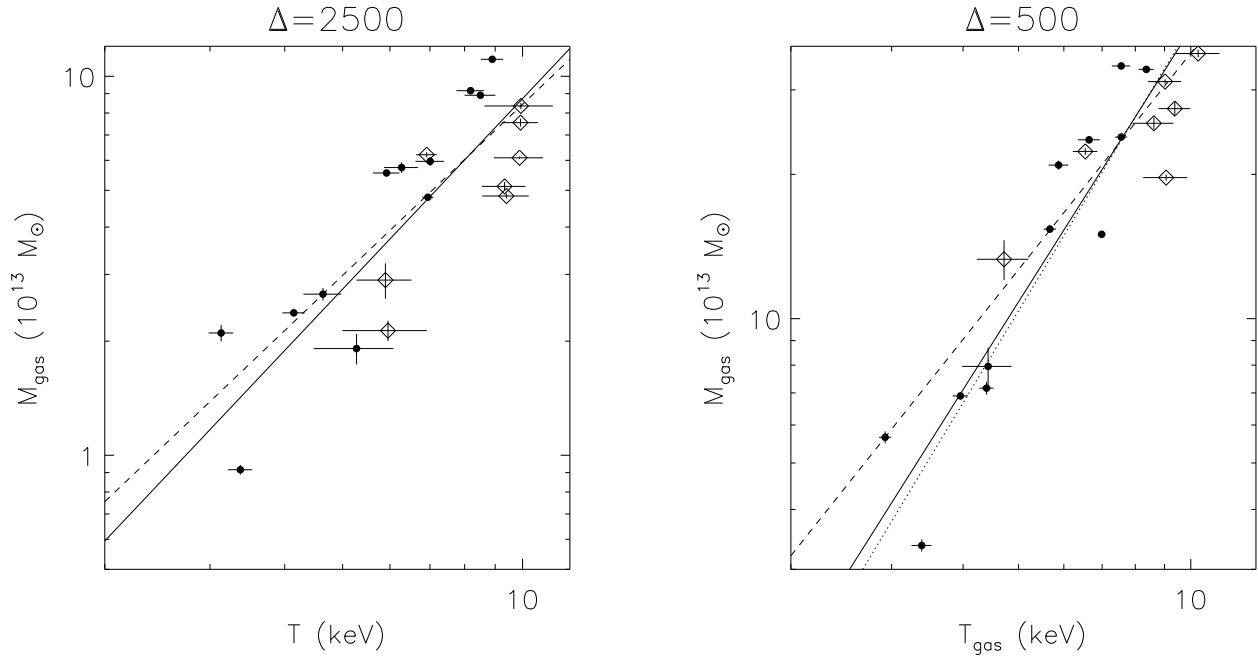


Fig. 10. (Left panel) $M_{\text{gas}} - T$ relation. The solid line represents the best-fit slope of $1.91(\pm 0.29)$; the dashed line is obtained fixing the slope to $3/2$. *Filled circles* represent CF galaxy clusters, whereas *open squares* are NCF objects. (Right panel) $M_{\text{gas}} - T_{\text{ew}}$ relation. The solid line represents the best-fit $M_{\text{gas},13} = 0.52(\pm 0.19) \times T_{\text{ew}}^{1.89(\pm 0.20)}$; the dashed line is obtained fixing the slope to $3/2$. The dotted line represents the best-fit results in Mohr et al. (1998).

(Arnaud & Evrard 1999, Viklinhin et al. 1999). This propagates directly to the $M_{\text{gas}} - T$ relation in the following way: $M_{\text{gas}} \approx f_{\text{gas}} M_{\text{tot}} \propto T^{3/2+\alpha}$, where a dependence of the form $f_{\text{gas}} \propto T^\alpha$ is introduced. In Fig. 9 and Table 4, we show that there is a slightly positive correlation between f_{gas} and T , with a slope larger than 0 by 1.9σ both at $\Delta = 2500$ and 1000 . As a consequence of this, the $M_{\text{gas}} - T$ relation (Fig. 10) tends to show a slope larger than 1.5.

Fitting with a power law the outer X-ray emission, Vikhlinin, Forman & Jones (1999) found that $M_{\text{gas}} \propto T^{1.71 \pm 0.13}$ (at the baryon overdensity of $1000 \approx 200$ in the dark matter overdensity). From the observed $L - T$ relation and applying X-ray scaling laws, Neumann & Arnaud (2001) found that $M_{\text{gas}} \propto T^{1.94}$ is required. Mohr, Mathiesen & Evrard (1999) estimated in a sample of nearby galaxy clusters that $M_{\text{gas}} \propto T^{1.98 \pm 0.18}$ within a density contrast of 500. At this overdensity, our sample includes 19 galaxy clusters, of which only two are directly observed (see Fig. 1). If we extrapolate the physical quantities as described in Section 4, we obtain the correlation plotted in Fig. 10 (right panel) that shows an agreement in the overall trend with a slope of $1.89(\pm 0.20)$.

It is worth noting that, while at an overdensity of 2500 there is a considerable segregation between CF and NCF systems, when going out to $\Delta = 500$ the segregation disappears. This kind of behaviour is in line with expectations indeed, while at $\Delta = 2500$ the CF region contributes substantially to the overall gas mass, at $\Delta = 500$ the contribution is quite small. The fact that segregation is actually not observed in our data at

an overdensity of 500 indicates that the extrapolations made to derive quantities at $\Delta = 500$ are reasonable ones.

5.3. $L - T$ relation

The self-similar dependence between luminosity and temperature is written as

$$\begin{aligned}
 L &\approx \epsilon \text{Vol} \approx \Lambda(T) n_{\text{gas}}^2 R^3 \\
 &\approx f_{\text{gas}}^2 T^{1/2} M_{\text{tot}}^2 R^{-3} \approx H_z^2 \Delta f_{\text{gas}}^2 T^{1/2} M_{\text{tot}} \\
 &\approx H_z \Delta^{1/2} f_{\text{gas}}^2 T^2,
 \end{aligned} \tag{14}$$

where ϵ is the X-ray emissivity and several, but reasonable, assumptions are made. Specifically: the cooling function, $\Lambda(T)$, is here described by only bremsstrahlung emission that is strictly valid only for $T > 2$ keV; the gas fraction, f_{gas} , and the radial dependence in the volume, $\text{Vol} \approx r_\Delta^3$, are not dependent on the temperature (see, e.g., Arnaud & Evrard 1999).

On the other hand, observations of the X-ray properties in cluster samples did show a departure from the predicted slope of 2 with a measured value of about 3 (Mushotzky 1984, Edge & Stewart 1991, David et al. 1993) and a scatter along the mean relation that can be reduced considering properly the effect of the cool cores (Fabian et al. 1994). Once the impact of the strength of cooling flows on the measured luminosity and emission-weighted temperature is taken into account, the $L - T$ correlation is shown to be tighter and more, but still not completely, consistent with the self-similar prediction (Allen & Fabian 1998, Markevitch 1998, Arnaud & Evrard 1999, Ettori,

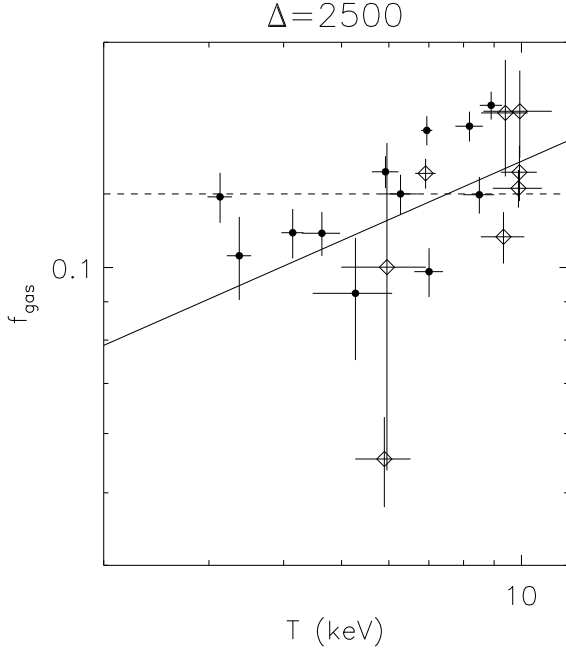


Fig. 9. $f_{\text{gas}} - T_{\text{mw}}$ relation. The solid line represents the best-fit slope of $0.61(\pm 0.31)$; the dashed line is obtained fixing the slope to 0. *Filled circles* represent CF galaxy clusters, whereas *open squares* are NCF objects.

Allen & Fabian 2001). However, a steeper $L - T$ dependence is expected when this relation is investigated over one order of magnitude in temperature, if the intracluster gas was pre-heated before the accretion in the potential well rising the entropy level in cooler systems (e.g. Ponman et al. 1996; Cavaliere, Menci & Tozzi 1997; Ponman, Cannon & Navarro 1999; Tozzi & Norman 2001). Gas-dynamic simulations (e.g. Bialek, Evrard & Mohr 2001, Borgani et al. 2002) are capable of recovering the observed slope once the effect of non-gravitational heat input from, e.g., AGNs and supernovae in the order of about 100 keV cm^2 , released either in an impulsive way or during the cluster formation history according to the star formation rate, is taken into account.

In the temperature range investigated here, we observe a slope that is slightly higher, but still consistent within 2σ , with 2 using any of the three definitions of T (see Table 4) and at any overdensity (cf. Fig. 7).

5.4. $L - M$ relation

From the observed correlation between total mass and gas temperature and between X-ray luminosity and temperature, it is straightforward to derive the dependence between gas luminosity and total mass. Combining eqn. 11 and 14, we obtain that

$$L \approx H_z^2 \Delta f_{\text{gas}}^2 T^{1/2} M_{\text{tot}} \quad (15)$$

Using a sample of 106 clusters observed with *ROSAT* PSPC in the energy range 0.5–2.0 keV and with total masses es-

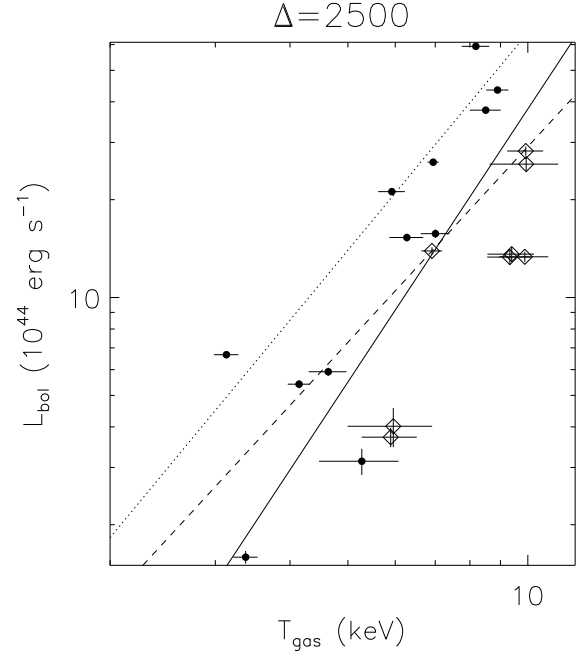


Fig. 11. $L - T_{\text{mw}}$ relation. The solid line represents the best-fit slope of $2.79(\pm 0.55)$; the dashed line is obtained fixing the slope to 2. *Filled circles* represent CF galaxy clusters, whereas *open squares* are NCF objects. The dotted line shows the best-fit from Allen et al. (2001), that follows the distribution of the CF clusters in our sample.

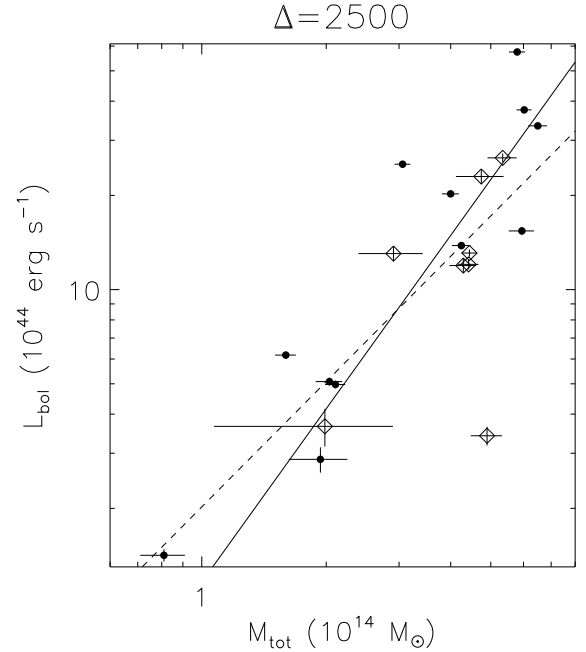


Fig. 12. $L - M$ relation. The solid line represents the best-fit slope of $1.54(\pm 0.26)$; the dashed line is obtained fixing the slope to $4/3$. *Filled circles* represent CF galaxy clusters, whereas *open squares* are NCF objects.

timated through the β -model, Reiprich & Böhringer (2002) measure a slope of $1.80(\pm 0.08)$ in the $L_{\text{bol}} - M_{200}$ relation. This value is marginally consistent with our results enclosed between $1.84(\pm 0.23)$, at $\Delta = 2500$, and $1.28(\pm 0.15)$, at $\Delta = 1000$ (cf. Table 4 and Fig. 7). These values lie between $4/3$, as predicted in the self-similar scenario, and $11/6$, that is expected for a ‘minimum-entropy’ scenario in which cluster cores maintain signature of an earlier galaxy formation activity (cf. Evrard & Henry 1991).

It is worth noticing that to use the X-ray galaxy clusters as cosmological probes and constraining the cluster mass function, the $L - T$ and $M - T$ relations are generally applied to recover from the observed X-ray luminosity a corresponding mass. For a given luminosity, L , this procedure carries an intrinsic scatter on the estimated mass, $\sigma_{\log M}$, that is the convolution of the scatter on the temperature originated in the $L - T$ relation, $\sigma_{\log T}$, with that present in the $M - T$ relation. From our estimates, this intrinsic scatter is about 0.20 to be compared with the observed scatter in the $L - M$ relation of 0.14, that is about 30 per cent less (we have considered results for emission-weighted temperatures at the overdensity of 2500; these values are 0.24 and 0.20 at $\Delta = 1000$, respectively). As a consequence of that, the direct application of the $L - M$ relation as tight as observed provides a more robust way to infer the cluster masses from large X-ray surveys (see also discussion on the cluster mass function estimated using the $L - M$ relation in Reiprich & Böhringer 2002).

6. Summary and Conclusions

We have used resolved gas temperature and density profiles obtained from direct deprojection of *BeppoSAX* spectral data to measure the gravitating mass profiles of 20 nearby ($0.010 < z < 0.103$; median redshift of 0.050) clusters. This sample is, to date, the largest for which the physical quantities have all been obtained from the same dataset.

At the overdensity (with respect to the critical density at a given redshift) of 2500, where 18 galaxy clusters in our sample have an observed temperature and luminosity, their gas mass weighted temperature spans over a factor of three in mass-weighted temperature ($3.1 \text{ keV} < T_X < 9.9 \text{ keV}$; median value: 6.9 keV) and two orders of magnitude in luminosity ($1.7 \times 10^{44} \text{ erg s}^{-1} < L_X < 6.1 \times 10^{45} \text{ erg s}^{-1}$; median value: $1.5 \times 10^{45} \text{ erg s}^{-1}$). We recover the total gravitating mass adopting either a King or a NFW functional form of the potential well. We obtain that the X-ray mass estimates are generally in good agreement with optical measurements. After a selection that includes in the analyses only systems with positive total mass at the 95 per cent level of confidence for a given overdensity Δ , we investigate in a consistent and robust way several correlations present between the quantities observed and derived from the X-ray analysis. Considering the high thermal energy associated with these objects, we are in the conditions to investigate the galaxy cluster scaling laws excluding systematics related to the energetic budget, but including statistical errors propagated from spatially-resolved gas density and temperature profiles.

Considering two subsamples of clusters with (CF; 12 objects) and without (NCF; 8 obj.) a mass deposition rate in the core (note that we do not consider any multi-phase gas in our spectral analysis, so that this classification only individuate systems more –CF– or less –NCF– relaxed), we observe a segregation in the correlation planes according to this classification as originally suggested from Fabian et al. (1994) on the $L - T$ relation. Moreover, the scatter measured in these relations is reduced when only CF systems are considered. These results point out an intrinsic scatter that is generally present in these correlations and is due to the dynamical status of the objects in exam. As expected, the scatter is greater for relations computed at larger overdensities, i.e. smaller radii, where the contribution from the more concentrated gas density is larger.

For each scaling relation that we investigate in the present work, we summarize here our main results:

- **$M - T$ relation:** at any overdensity, the slope is consistent with a value of 1.5. In particular, we obtain the best-fit robust relations $M_{14} = 0.20(\pm 0.08) \times T_{\text{mw}}^{1.54(\pm 0.22)}$ and $M_{14} = 0.25(\pm 0.09) \times T_{\text{mw}}^{1.5}$ at $\Delta = 2500$. A segregation between CF and NCF clusters is observable. When the slope is fixed to 1.5, the scatter is reduced by about 30 per cent for only CF objects ($\Delta = 2500$). The normalization is lower than the results of hydrodynamic simulations, but the large scatter observed makes large the uncertainties that we measure. In the same direction, the results on the $R - T$ relation show a slope in agreement with what is obtained in numerical simulations and a normalization slightly lower ($R_{100} = 3.27(\pm 0.41) \times T_{\text{mw}}^{0.47(\pm 0.07)}$ and $R_{100} = 3.19(\pm 0.32) \times T_{\text{mw}}^{0.5}$). The evidence for a strong correlation between the fitted parameters in the $M - T$ relation suggests that the physical interpretation of steeper slopes and lower normalizations can be misleading if the degeneracy between these quantities is not properly taken into account.
- **$M_{\text{gas}} - T$ relation:** both at $\Delta = 2500$ and 1000, we observe a marginally significant trend between the gas mass fraction and the temperature (best-fit slope: 0.61 ± 0.31 at $\Delta = 2500$). As a consequence of that, there is evidence, significant at less than 2σ , that the slope in the $M_{\text{gas}} - T$ relation is different (and more steep) than the one present in the $M - T$ relation. At $\Delta = 2500$, we measure a slope of $1.91(\pm 0.29)$. Due to the observed segregation between relaxed and not-relaxed clusters, the scatter is reduced by 20 per cent when CF objects are considered.
- **$L - T$ relation:** our results are consistent with a slope of 2 as predicted from the scaling law relations (maximal deviation of 2.1σ at $\Delta = 1500$). At the overdensity of 2500, we measure $L_{44} = 0.06(\pm 0.06) \times T_{\text{mw}}^{2.79(\pm 0.55)}$ and $L_{44} = 0.29(\pm 0.22) \times T_{\text{mw}}^2$. The scatter is lowered by 20 per cent when only CF galaxy clusters are considered.
- **$L - M$ relation:** the central value measured on the slope of this relation varies between the self-similar and the ‘minimum-entropy’ prediction. The scatter in the relation is reduced by 25 per cent when only CF clusters are con-

sidered. We notice that the direct application of the $L - M$ relation as tightly as observed provides a more robust way (in other words, less scatter is propagated) to infer the cluster masses from large X-ray surveys than the combined application of the $L - T$ and $M - T$ relations.

In a forthcoming paper (Ettori et al., in preparation), the cosmological implications of these relations and of the gas mass fraction distribution observed at different overdensity will be investigated.

Acknowledgements

This paper has made use of linearized event files produced at the *BeppoSAX* Science Data Center. We thank the referee, Dr. K. Mitsuda, for several suggestions that helped us to improve the presentation of this work. Jukka Nevalainen is thanked for useful comments.

References

- Afshordi N., Cen R., 2002, *ApJ*, 564, 669
- Allen S.W., Fabian A.C., 1998, *MNRAS*, 297, L57
- Allen S.W., Schmidt R.W., Fabian A.C., 2001, *MNRAS*, 328, L37
- Arnaud K.A., 1996, "Astronomical Data Analysis Software and Systems V", eds. Jacoby G. and Barnes J., ASP Conf. Series vol. 101, 17
- Arnaud M., Evrard A.E., 1999, *MNRAS*, 305, 631
- Bialek J.J., Evrard A.E., Mohr J.J., 2001, *ApJ*, 555, 597
- Binney, J. & Tremaine, S., 1987, *Galactic Dynamics*, Princeton University Press, p. 226f
- Boella G., Butler R.C., Perola G.C., Piro L., Scarsi L., Bleeker J.A.M., 1997, *A&AS*, 112, 299
- Borgani S., Governato F., Wadsley J., Menci N., Tozzi P., Quinn T., Stadel J., Lake G., 2002, *MNRAS*, in press (astro-ph/0205471)
- Bryan G.L., Norman M.L., 1998, *ApJ*, 495, 80
- Buote D.A., 2000, *ApJ*, 539, 172
- Cavaliere A., Fusco-Femiano R., 1976, *A&A*, 49, 137
- Cavaliere A., Menci N., Tozzi P., 1997, *ApJ*, 484, L21
- D'Acri F., De Grandi S., Molendi S., 1998, in "The Active X-ray Sky: Results from *BeppoSAX* and *RXTE*", Active X-ray Sky symposium, L. Scarsi, H. Bradt, P. Giommi and F. Fiore eds., Elsevier, Amsterdam
- David L.P., Forman W. & Jones C., 1991, *ApJ*, 380, 39
- David L.P., Slyz A., Jones C., Forman W., Vrtilik S.D., & Arnaud K.A., 1993, *ApJ*, 412, 479
- David L.P., Nulsen P.E.J., McNamara B.R., Forman W., Jones C., Ponman T., Robertson B., Wise M., 2001, *ApJ*, 557, 546
- De Grandi S., Molendi S., 2001, *ApJ*, 551, 153
- De Grandi S., Molendi S., 2002, *ApJ*, 567, 163
- Dickey J.M., Lockman, F.J., 1990, *ARA&A*, 28, 215
- Edge A.C., Stewart G., 1991, *MNRAS*, 252, 414
- Ettori S., Fabian A.C., 1999, *MNRAS*, 305, 834
- Ettori S., 2000, *MNRAS*, 311, 313
- Ettori S., Allen S.W., Fabian A.C., 2001, *MNRAS*, 322, 187
- Ettori S., Fabian A.C., Allen S.W., Johnstone R.M., 2002, *MNRAS*, 331, 635
- Evrard A.E., Henry J.P., 1991, *ApJ*, 383, 95
- Evrard A.E., Metzler C.A., Navarro J.F., 1996, *ApJ*, 469, 494
- Fabian A.C., 1994, *ARAA*, 32, 227
- Fabian A.C., Crawford C.S., Edge A.C., Mushotzky R.F., 1994, *MNRAS*, 267, 779
- Ferretti L., Dallacasa D., Govoni F., Giovannini G., Taylor G.B., Klein U., 1999, *A&A*, 344, 472
- Finoguenov A., Reiprich T.H., Böhringer H., 2001, *A&A*, 368, 749
- Girardi M., Giuricin G., Mardirossian F., Mezzetti M., Boschin W., 1998, *ApJ*, 505, 74
- Henriksen M.J., Markevitch M., 1996, *ApJ*, 466, L79
- Henry J.P., Arnaud K.A., 1991, *ApJ*, 372, 410
- Horner D.J., Mushotzky R.F., Scharf C.A., 1999, *ApJ*, 520, 78
- Hjorth J., Oukbir J., van Kampen E., 1998, *MNRAS*, 298, 1
- Jansen F. et al., 2001, *A&A*, 365, L1
- Jing Y.P., Suto Y., 2000, *ApJ*, 529, L69
- Johnstone R.M., Allen S.W., Fabian A.C., Sanders J.S., 2002, *MNRAS* submitted (astro-ph/0202071)
- Kaastra J.S., 1992, *An X-Ray Spectral Code for Optically Thin Plasmas* (Internal SRON-Leiden Report, updated version 2.0)
- Kaiser N., 1986, *MNRAS*, 222, 323
- King I.R., 1962, *AJ*, 67, 471
- Krisz G.A., Cioffi D.F., Canizares C.R., 1983, *ApJ*, 272, 439
- Ikebe Y., Reiprich T.H., Böhringer H., Tanaka Y., Kitayama T., 2002, *A&A*, in press (astro-ph/0112315)
- Liedahl D.A., Osterheld A.L., Goldstein W.H., 1995, *ApJ*, 438, L115
- Markevitch M., 1998, *ApJ*, 504, 27
- Markevitch M., Vikhlinin A., Forman W.R., Sarazin C.L., 1999, *ApJ*, 527, 545
- Matsushita K., Belsole E., Finoguenov A., Böhringer, 2002, *A&A*, in press (astro-ph/0201242)
- McLaughlin D.E., 1999, *AJ*, 117, 2398
- Mohr J.J., Mathiesen B., Evrard A.E., 1999, *ApJ*, 517, 627
- Molendi S., De Grandi S., Fusco-Femiano R., 2000, *ApJ*, 533, L43
- Molendi S., Pizzolato F., 2001, *ApJ*, 560, 194
- Mushotzky R.F., 1984, *Phys. Scr.*, T7, 157
- Navarro J.F., Frenk C.S., White S.D.M., 1995, *MNRAS*, 275, 720
- Navarro J.F., Frenk C.S., White S.D.M., 1997, *ApJ*, 490, 493
- Nevalainen J., Markevitch M., Forman W., 2000, *ApJ*, 536, 73
- Neumann D.M., Arnaud M., 1999, *A&A*, 348, 711
- Neumann D.M., Arnaud M., 2001, *A&A*, 373, L33
- Peres C.B., Fabian A.C., Edge A.C., Allen S.W., Johnstone R.M., White D.A., 1998, *MNRAS*, 298, 416
- Ponman T.L., Bourner P.D.J., Ebeling H., Böhringer H., 1996, *MNRAS*, 283, 690
- Ponman T.L., Cannon D.B., Navarro J., 1999, *Nature*, 397, 135
- Press W.H., Schechter P., 1974, *ApJ*, 187, 425
- Press W.H., Teukolsky S.A., Vetterling W.T., Flannery B.P., 1992, *Numerical Recipes*, Cambridge University Press
- Reiprich T.H., Böhringer H., 2002, *ApJ* in press (astro-ph/0111285)
- Sanders J.S. & Fabian A.C., 2002, *MNRAS*, in press (astro-ph/0109336)
- Sarazin C.L., 1988, *X-ray emission from clusters of galaxies*, Cambridge University Press
- Schindler S., 1996, *A&A*, 305, 756
- Tamura T. et al., 2001, *A&A*, 365, L87
- Tanaka T., Inoue H. & Holt S.S., 1994, *PASJ*, 46, L37
- Thomas P.A., Muanwong O., Pearce F.R., Couchman H.M.P., Edge A.C., Jenkins A., Onoura L., 2001, *MNRAS*, 324, 450
- Tozzi P., Norman C., 2001, *ApJ*, 546, 63
- Vikhlinin A., Forman W., Jones C., 1999, *ApJ*, 525, 47
- Weisskopf M.C., Tanabaum H.D., Van Spebroeck L.P., O' Dell S.L., 2000, *Proc SPIE* 4012, in press (astro-ph/0004127)